2554–2565 Nucleic Acids Research, 2012, Vol. 40, No. 6 Published online 1 December 2011
doi:10.1093/nar/gkr1109

Metastases suppressor NME2 associates with telomere ends and telomerase and reduces telomerase activity within cells

Anirban Kar[1], Dhurjhoti Saha[1], Gunjan Purohit[1], Ankita Singh[1], Parveen Kumar[2], Vinod Kumar Yadav[2], Pankaj Kumar[2], Ram Krishna Thakur[1] and Shantanu Chowdhury[1,2,*]

[1]Proteomics and Structural Biology Unit and [2]G.N.R. Knowledge Centre for Genome Informatics, Institute of Genomics and Integrative Biology, CSIR, Mall Road, Delhi 110 007, India

Received June 27, 2011; Revised November 4, 2011; Accepted November 5, 2011

ABSTRACT

Analysis of chromatin-immunoprecipitation followed by sequencing (ChIP-seq) usually disregards sequence reads that do not map within binding positions (peaks). Using an unbiased approach, we analysed all reads, both that mapped and ones that were not included as part of peaks. ChIP-seq experiments were performed in human lung adenocarcinoma and fibrosarcoma cells for the metastasis suppressor non-metastatic 2 (NME2). Surprisingly, we identified sequence reads that uniquely represented human telomere ends in both cases. *In vivo* presence of NME2 at telomere ends was validated using independent methods and as further evidence we found intranuclear association of NME2 and the telomere repeat binding factor 2. Most remarkably, results demonstrate that NME2 associates with telomerase and reduces telomerase activity *in vitro* and *in vivo*, and sustained NME2 expression resulted in reduced telomere length in aggressive human cancer cells. Anti-metastatic function of NME2 has been demonstrated in human cancers, however, mechanisms are poorly understood. Together, findings reported here suggest a novel role for NME2 as a telomere binding protein that can alter telomerase function and telomere length. This presents an opportunity to investigate telomere-related interactions in metastasis suppression.

INTRODUCTION

Eukaryotic chromosome ends are protected by nucleoprotein assemblies called telomeres that are critical for maintaining chromosome integrity. In humans, telomeres comprise double-stranded DNA having short-tandem repeats of 5′-TTAGGG-3′ that extend into single strand G-rich overhang of ~130–210 nt at the 3′-end (1,2). Though the exact mechanism of how telomeres stabilize chromosome ends is not well established, it is increasingly becoming evident that regulatory control of telomerase activation (and/or recruitment to telomere ends) involves participation and cross-talk between telomerase and established telomeric protein complexes, including telomere repeat binding factors 1 and 2 (TRF1 and TRF2), protection of telomere 1 (POT1), TRF1/TRF2 interacting factor (TIN2), TPP1 and hRAP1 (3,4).

In most human somatic cells ~50–100 nt are lost from the telomere end during each replication cycle, and shortening of telomeres below a critical length signals apoptosis (5). In contrast, telomere length is restored in human cancer and germ cells by telomerase, thereby maintaining cell proliferation and tumorigenicity (6,7). Telomerase is a ribonucleoprotein, composed of catalytic telomerase reverse transcriptase (TERT) enzyme unit and telomerase RNA (TER), which is used as a template during telomere elongation (8,9). The contrasting nature of telomere maintenance in human tumours vis-à-vis somatic cells is due to the presence of telomerase, which is otherwise suppressed in somatic cells. Telomerase level has been correlated with progression of several cancer types, including acute leukaemia, breast, prostate, lung and melanoma (10). Although the impact of telomerase in development of cancer has been extensively studied, its role in invasiveness

*To whom correspondence should be addressed. Tel: +91 11 2766 6157; Fax: +91 11 2766 7471; Email: shantanuc@igib.res.in

of tumour cells and metastasis are poorly understood (11,12). Telomere elongation was noted in metastatic mouse tumour cells (13) in line with the observation that though telomere dysfunction initiates carcinogenesis, telomerase-mediated telomere maintenance is crucial for sustaining metastasis (11). Indeed suppression of telomerase activity in tumour-bearing mice was found to significantly reduce metastatic progression (12,14).

In this context, the metastasis suppressor non-metastatic 2 (NME2, also known as nm23-H2) is of interest. Comparison of seven murine K-1735 melanoma-derived cell lines with differing metastatic potential led to identification of the *nm23* gene whose low expression was associated with highly invasive cells (15). This finding provided first evidence that a single gene could modulate the invasive phenotype—'coining' the idea of metastases suppressor factors. Human *nm23* has 10 known isoforms, H1–H10, and of these H1 (or NME1) and H2 are the best studied (16–19). Involvement of NME2 in metastases has been demonstrated, where overexpression resulted in reduced metastasis of human oral squamous carcinoma, breast carcinoma and murine melanoma cells (20–22). Moreover, NME2 expression was found to negatively correlate with advanced/metastatic stages across several tumour types (23). However, mechanisms underlying anti-metastatic function of NME2 are still poorly understood.

Herein, following analysis of NME2 ChIP-seq peaks, we identified *in vivo* binding of NME2 to human telomere ends. Based on this, we focused on confirming NME2 association with telomeres *in vivo* and its relevance to function. The results demonstrate NME2 as a telomere repeat binding factor (TRF), which associates with telomerase both *in vitro* and *in vivo* and limits telomerase activity and telomere length in cancer cells. These functions of NME2 suggest its role as a modulator of telomere length, which to our understanding has not been observed earlier for any metastases suppressor. Together, these observations suggest novel biological functions of NME2, which may play a key role in understanding metastatic outcome in the context of telomerase activity.

MATERIALS AND METHODS

Cells and culture conditions

A549 cells were obtained from the national repository of cell lines at National Centre for Cell Sciences (NCCS), Pune, India, and maintained in Dulbecco's Modified Eagle medium (DMEM) supplemented with 10% foetal bovine serum at 37°C in 5% CO_2. HT-1080 cells were obtained from the American type cell culture (ATCC, USA) and maintained in Modified Eagle medium (MEM) with Earles modification and supplemented with 10% foetal bovine serum at 37°C in 5% CO_2.

Chromatin immunoprecipitation

ChIP assays were performed as per protocol provided by Upstate Biotechnology with modifications as suggested in Fast ChIP protocol (24). After 48 h of transfection of pcDNA-NME2 with MYC tag using Lipofectamine 2000 (Invitrogen), antibody against the MYC epitope (Sigma clone 9E10) was used to immunoprecipitate chromatin in A549 and HT-1080 cells. Mouse IgG was used for mock immunoprecipitation in all the cell lines. Briefly, cells were fixed with 1% formaldehyde for 10 min and lysed. Chromatin was sheared to an average size of ~500 bp using a Misonix 3000 sonicator. Twenty-five per cent of lysate was used to isolate input chromatin using phenol–chloroform and ethanol precipitation. Lysate was precleared using protein-A sepharose beads, and ChIP was performed using 5 µg of the respective antibody incubated overnight at 4°C. Immune complexes were collected using herring sperm DNA-saturated protein-A Sepharose and washed extensively. Chelex-100 resin was used to extract DNA from immunoprecipitated chromatin as described previously (24).

Illumina library construction and sequencing

NME2-bound DNA from A549 and HT-1080 cells expressing MYC-tagged NME2 was quantified, and 10 ng from each sample was taken for end repair using Illumina sample preparation kit. Samples were purified using PCR purification kit (Qiagen, Germany). Thereafter 'A' base was added to the samples 3′-end using Illumina sample preparation kit. After the end of the reaction, samples were again purified by PCR purification kit (Qiagen). Then flow-cell primer specific adapters were ligated to the ChIP DNA fragments and samples were further purified by MinElute columns. Size selection was done after adapter ligation using 2% agarose gel. Gel extraction columns (Qiagen) were used to purify DNA fragments ranging between 150 and 350 bases. These eluted samples were then purified using MinElute columns and these samples were then amplified for 18 cycles to enrich adapter-ligated DNA fragments. After PCR purification and elution the DNA was quantified using Picogreen method, and then 3.5 pico moles of each sample was sequenced on GAII (Illumina, USA) according to manufacturer's protocol.

We extracted 36 base sequence reads from the resulting image files using the open source Firecrest and Bustard applications on 288-node HP Cluster Platform 3000 running Linux with XC System Software and Sun Microsystems 24 core server. Reads were trimmed to 5′-end 24 bases to minimize inclusion of sequencing errors typically found within the last few bases towards the 3′-end of reads. All reads were mapped to the unmasked human genome hg18 using the MAQ program (25) allowing two mismatches.

Peak generation

To find NME2 binding sites, the resulting mapped reads were processed using CisGenome as described earlier (26). Briefly, CisGenome uses a conditional binomial model to identify regions in which the ChIP reads are significantly enriched relative to the control reads. We assigned 10% FDR cut-off (26) to generate NME2-ChIP binding sites. In order to filter out low-quality sites we applied two post-processing options boundary refinement and single-strand filtering (26). For analysis of occurrence

and enrichment of reads containing Tel_{rep}, we used the 36 bp reads as obtained from sequencing, where Tel_{rep} units were searched in the first 30 bases to avoid anomalies due to error-prone sequencing at the 3′-ends.

Generation of simulated reads: promoter and ENCODE regions

We selected ±5 kb region (with respect to TSS) of 20 663 protein coding genes. Five regions of 100 bp each were randomly selected from each 10-kb region and used to generate 50 fragments of 30-bp length (scheme given in Supplementary Methods) such that the fold-coverage was as similar to that found for overall binding positions of NME2 ChIP-seq peaks (~14.8-fold). This resulted in a total of ~5.16 million reads (at 15-fold coverage). TTAG GG/CCCTAA sequence patterns with up to one mismatch were searched within these reads. In a similar way, 30 Mb of ENCODE region were selected representing 44 genomic regions from the whole genome (27). Each genomic region was further distributed into windows of 10 kb. From each 10-kb window, seven genomic regions of 500 bp were randomly selected and used to generate 250 fragments of 30-bp length. Total 5.25 million reads were obtained at 15-fold coverage and used to find the occurrence of telomere repeat units GGGTTA/CCCTAA with up to one mismatch.

Dot blot analysis

For dot blot analysis, ChIP DNA was denatured at 95°C and dot blotted on hybond membrane (Amersham) in 2X SSC buffer. Membranes were pre-hybridized in Rapid-Hyb buffer (Amersham) for 15 min. Following this, hybridization with a 900-bp radio-labelled telomeric probe $(TTAGGG)_n$ or 418-bp radio-labelled ALU probe (Supplementary Information) was performed for 3 h at 65°C and membranes washed with 2X SSC and 0.1% SDS three times before exposing overnight on phosphoimager imaging plate. All data were scanned using FUJI Phosphoimager FLA2000. Data was processed and quantified using Multigauge image analysis software.

Immunofluorescence microscopy

Cells were grown overnight on cover slips and transfected with GFP-NME2. After 36 h cells were fixed in 4% paraformaldehyde for 20 min at 37°C in a water bath. Samples were blocked with blocking buffer (1X PBS, 1% BSA, 0.5% Triton X-100, 0.05% Tween 20) containing 10% goat serum for 30 min at 37°C and then incubated with anti-TRF2 (NB110-57130, Novus Biologicals) or anti-hTERT Y182 (ab32020, Abcam, USA) for 2 h at 37°C. After washing by 1X PBS, samples were incubated with secondary antibody conjugated with alexa-594 (Molecular probes, USA). Nuclei were counterstained with 4, 6-diamidino-2 phenylindole (DAPI) (Santacruz, USA). All images were collected with Nikon eclipse-Ti wide-field fluorescence microscope (Apochromat Pluar 60X oil objective lenses) and corrected for background using Nikon NIS elements AR software. Further analysis for image co-localization and Pearsons's correlation were obtained using Nikon NIS elements AR software.

Preparation of nuclear extracts

A549 and HT-1080 cells grown in DMEM media supplemented with 10% FBS (Sigma, USA) were collected and washed in cold 1X PBS and nuclear extract was isolated using nuclear extract kit (Cell Extract from Sigma, USA) as per manufacturer protocol.

Immunoprecipitation

For immunoprecipitation experiments, 1 mg of nuclear extract was incubated for 2 h at 4°C with 6 µg of anti-NME2 antibody (MC-412 Kamiya Biomedical Company, USA), anti-telomerase reverse transcriptase antibody (Y182; ab32020 Abcam) or anti-TRF2 (NB110-57130 Novus Biologicals), and immunoprecipitation was performed using Catch and Release co-immunoprecipitation kit (Millipore, USA) as per manufacturer's protocol. Antibody used for NME2 did not cross react with NME1 (Supplementary Figure S2). Where indicated RNase-A, ethidium bromide or DNase I was included during the incubation at 0.1 mg/ml. For NME1 ChIP and western-blotting, anti-NME1 antibody (MC-382, Kamiya Biomedical Company) was used.

Antibodies and western blotting

For western analysis, immunoprecipitated nuclear extract were separated by sodium dodecyl sulphate-polyacrylamide gel electrophoresis (SDS–PAGE) and transferred to polyvinylidene difluoride membranes (Immobilon FL, Millipore); following primary and secondary antibodies were used for immuno-blotting. Primary antibodies anti-TRF2 (Novus Biologicals) and telomerase reverse transcriptase, hTERT (Y182; Abcam) and secondary antibodies, anti-mouse and anti-rabbit alkaline phosphatase conjugated were from Sigma.

Recombinant NME2 and $NME2^{K12A}$ expression

Recombinant NME2 and mutant (K12A) were expressed in *Escherichia coli* using the pRSETA-NME2 clones (28) and purified using Ni–NTA chromatography to obtain His-tagged protein, which was used for all pull-down experiments (Supplementary Figure S1). In an independent preparation His-tag was removed, resin bound protein was cleaved (0.6 µg of enterokinase per 25 µg of fusion protein in reaction buffer (50 mM Tris pH 8.0, 5 mM $CaCl_2$) and subsequently enterokinase was removed using enterokinase removal kit (Sigma, USA). NME2 without His-tag gave comparable results as the His-tagged product in all assays.

In vitro pull down assays

Bacterially expressed 6X His-tagged full-length NME2 was purified using Ni-NTA agarose beads (Qiagen) as described earlier (28); 1 µg of His-tagged protein on beads was used for each binding reaction. For pull-down

assays 1 mg of nuclear lysate was incubated with His-tagged protein for 1 h after preclearing with Ni-NTA beads. The mixtures were washed three times with NETN (20 mM Tris, pH 8.0, 100 mM NaCl, 0.5% Nonidet P-40 and 1 mM EDTA), eluted with 2X SDS buffer, resolved by SDS–PAGE, and transferred to polyvinylidene difluoride membranes (Immobilon Fl, Millipore) followed by analysis using respective primary and secondary antibodies.

Analysis of telomerase activity

Cells were lysed in a lysis buffer and telomerase-containing fraction was prepared for real-time telomerase activity assay using quantitative telomerase detection kit (US-Biomax, USA) according to the manufacturer's protocol. To examine the effect on telomerase activity, various concentrations of His-tagged NME2 or NME (K12A) were incubated for 10 min at 30°C before subjecting to telomerase extension. Total protein extract (1 μg) was used in each reaction. For stable cells with sustained NME2 or empty vector expression (control cells), an equal amount of lysate was taken and further used for the assay as mentioned above. All assays were performed in triplicate and relative fold-change in expression was calculated from the observed Ct values.

Flow cytometry for telomere length quantification

Analysis was performed using Telomere PNA Kit/FITC (DAKO) in a FACS Calibur flow cytometer (Becton Dickinson Immunocytometry Systems, San Jose, CA) using the FL1 channel for detection of fluorescein signal and the FL3 channel for propidium iodide. No compensation was set on the instrument. List mode data from 10^4 cells in each experiment was collected and analysed using CELL-Quest software (Becton Dickinson). The telomere fluorescence signal was defined as the mean fluorescence signal in G_0/G_1 cells after subtraction of the background fluorescence signal (i.e. FISH procedure without probe). Sample preparation and normalization was done as per manufacturer protocol. Experiments were performed using three independent preparations of either HA-NME2-expressing or control HA-vector-transformed cells maintained for up to 200 population doublings in each case.

RT–PCR for hTERT and NME2

RNA was extracted using TRIzol reagent (Sigma, USA) as per the manufacturer's protocol. Complementary DNA was synthesized using cDNA synthesis kit (Applied Biosystems, GMBH) following the manufacturer's instructions. Transcript levels were determined using the following primer set. NME2: fwd-CTGTCTTCACCACGTTCAGC, rev-GGCCTCTGAAGAACACCTGA. hTERT: fwd-GCCGATTGTGAACATGGACTACG, rev-GCTCGTAGTTGAGCACGCTGAA. β-Actin: fwd-TGCGTGACATTAAGGAGAAG, rev-CTGCATCCTGTCGGCAATG.

RESULTS

ChIP-seq for NME2 shows abundance of the telomere DNA motif

ChIP, followed by massive parallel sequencing, was performed in A549 lung adenocarcinoma cells for genomic binding positions of NME2. Because NME2 has several human homologs, MYC-tagged NME2 was expressed and immunoprecipitation was performed using antibody specific for MYC-tagged NME2, as reported earlier (28). NME2-immunoprecipitated samples were sequenced in duplicate at two ChIP-DNA concentrations in addition to mock sample for background correction; numbers of sequenced and mapped reads are given in Supplementary Table S1A. Using human reference genome sequence (hg18) >80% alignment of reads was achieved in the case of NME2-ChIP sample; overlapping reads were used for constructing NME2-binding positions (peaks) following background subtraction using published procedures (29). As a positive control, the only demonstrated binding site of NME2 (28,30–33) within the *c-myc* promoter was searched for and found in the constructed peaks. Surprisingly, close survey revealed several peaks with telomeric repeat (Tel_{rep}) units, TTAGGG or CCCTAA, and herein we have focused on this finding. We found 35 NME2-ChIP peaks of average length 250.6 bp with more than 70% identity with TTAGGG/CCCTAA stretch of same length (average identity = 88.2%, Supplementary Table S2A), wherein the observed average coverage of 200.8-fold was remarkably high relative to the 14.8-fold coverage observed overall for all NME2-peaks (Supplementary Table S1A). Figure 1A shows representative examples of peaks where all reads with perfect TTAGGG/CCCTTA (in red) are shown along with all other reads (blue).

Telomeric-repeat containing reads are unlikely to result from interstitial chromosome regions

Taking clue from this, for further analysis we considered all 36 bp reads that could be mapped within peaks and asked what fraction of the reads contained Tel_{rep} units. Either 4 or 3 6-mer units of TTAGGG/CCCTAA (after allowing 0/1 mismatch within each unit; in the following text we designate these units as $Tel_{rep\text{-}0/1}$) was searched within the first 30 bp. We reasoned that Tel_{rep} units are unlikely to result from promoter or other interstitial regions of the genome, where ChIP-seq binding analysis typically focuses on. Therefore, two control sets were made: (a) 10-kb region around transcription start sites of 20 663 unique human genes (~206.6 Mb) and (b) all ENCODE regions (30 Mb); 30-mer reads were randomly generated computationally [with coverage identical to that noted within NME2-ChIP peaks (methods)] and analysed for number of Tel_{rep} units. For every million ChIP-seq reads we found >9000 and >6000 reads, respectively, for replicate one and two, with four or three $Tel_{rep\text{-}0/1}$ units (Figure 1B and C). In contrast, on searching 5.17 million reads generated randomly from promoter regions, we found very few reads having Tel_{rep} units (2 and 65 reads with 4 Tel_{rep} units having 0 or 1 mismatch, respectively; 14

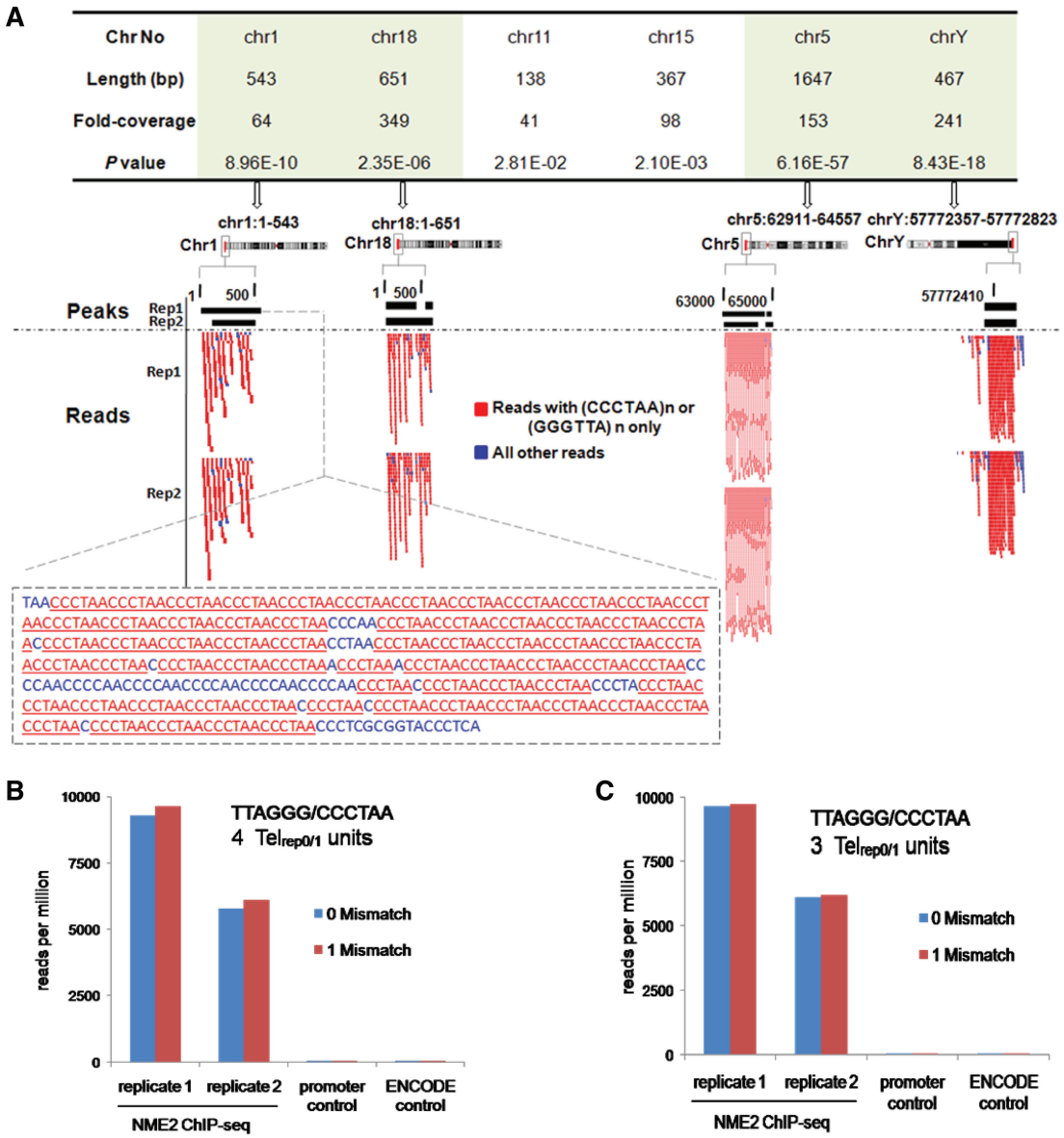

Figure 1. NME2-ChIP-seq peaks with telomere repeats. (**A**) Representative peaks that are made of almost entirely Tel_{rep} units—TTAGGG/CCCTAA. Lower panel shows reads (with or without Tel_{rep}) mapped to peaks; full sequence for one peak is shown below (non-Tel_{rep} reads in blue). Percentage identity is with respect to a stretch of TTAGGG/CCCTAA of similar length; fold-coverage is the ratio of total bp count of reads with Tel_{rep} that map within a peak over length of the peak. Supplementary Table S2A shows all peaks with Tel_{rep} units. Fraction of reads with either four Tel_{rep} (**B**) or three Tel_{rep} units (**C**) that mapped within NME2-ChIP peaks are shown in comparison to reads generated computationally from human promoter or ENCODE regions.

and 190 reads with 3 Tel_{rep} units with 0/1 mismatch, respectively). This was also true for 5.25 million reads made from ENCODE regions (4 and 26 reads with 4 Tel_{rep} units having 0/1 mismatch, respectively; 16 and 161 reads with 3 Tel_{rep} units with 0/1 mismatch, respectively). This clearly showed that a substantial number of tags harboured telomeric repeats and also that these tags are unlikely to result from promoters or interstitial genomic regions.

In order to validate the above results in a second cell line, ChIP-seq was performed using MYC-tagged NME2 in human fibrosarcoma HT1080 cells and analysed in the manner described above. Results were analogous to the ones obtained from A549 cells and are presented in Supplementary Tables S1B and S2B.

ChIP-seq algorithms typically focus on mappable regions (where reads can be placed at unique positions on the reference genome) of the genome and furthermore disregard regions that are not found to be enriched with reads vis-à-vis control samples for peak construction (29). We noted that telomeric repeats would be intrinsically limited in these aspects due to the repeating nature of the sequence, and found that roughly a third (~38%) of the Tel_{rep} reads did not map within designated NME2-ChIP positions. As above, we noted clear enrichment of reads with $Tel_{rep-0/1}$ in both replicates of NME2-ChIP relative to promoter or ENCODE regions (Supplementary Table S3A and S3B). Analysis of reads that do not constitute peaks, however, is with the caveat

that background signal from the mock sample is disregarded, since background correction is typically made during the peak generation process. On the other hand, multiple analytical protocols in the past have described surprisingly uneven representation of reads in control samples and prescribed this to various reasons, including chromatin accessibility, mappability of the genome and sample preparation for background correction (34,35). We noted that though relatively less (~30–35% lower compared to NME2 ChIP) there were many telomere repeats found in the IgG immunoprecipitated mock samples. It is possible that G/C-rich sequence and/or more accessibility at the chromosome ends makes telomeric-repeats relatively more amenable to chromatin pull-down. We reasoned that if one could use this information as lead and confirm using independent experiments, ChIP-seq would be useful to analyse binding to additional regions of the genome. Keeping this in mind, we devised experiments to test NME2 binding to telomere ends and its functional relevance.

NME2 binds to telomere ends *in vivo*

To confirm NME2 localization at telomere ends, we tested the intracellular association of NME2 with telomeric repeat DNA by chromatin immunoprecipitation (ChIP) using anti-NME2 antibody to immunoprecipitate protein-associated DNA fragments followed by dot blot analysis. Telomere-specific probes were hybridized to immunoprecipitated DNA in each case to detect association to telomeres. ChIP using anti-NME2 antibody was enriched for telomeric DNA relative to IgG (Figure 2A and B). Because NME1 and NME2 have 80% similarity at amino acid sequence level, in order to confirm NME2-specific localization we used MYC-tagged NME2, which was immunoprecipitated using an antibody-recognizing MYC epitope and gave clear enrichment in ChIP signal relative to IgG in the dot blot (Figure 2A and B). In contrast, ChIP against MYC-tagged NME1 using anti-MYC-tag antibody was not significantly enriched over its isotype control. We further used ChIP for TRF2 as a positive control in these experiments where a detectable signal was clearly visible. As a control for binding specificity, dot blots were hybridized with Alu sequences (Figure 2A, right panel). Further quantitation of the hybridized signals revealed that anti-MYC-tagged NME2 ChIP yielded about 42% (± 3; $n = 3$) of the total telomeric DNA in HT-1080 cells (Figure 2B) while TRF2 ChIP yielded about 58% (± 3; $n = 3$).

We additionally checked telomere-specific binding of NME2 using a PCR-based method demonstrated earlier. This method has been used earlier for telomeric DNA detection in several reports (36,37); typically, on PCR amplification, bands ranging from 50 to ~500 bp are observed signifying enrichment of telomeric fragments. DNA immunoprecipitated by anti-MYC tagged NME2, anti-TRF2 or anti-MYC tagged NME1 antibodies was PCR amplified using telomere-specific primers. We observed, as expected a clear enrichment of PCR signal in the anti-NME2 and TRF2 ChIP sample between 50 bp and ~500 bp relative to the control sample where a specific isotype antibody was used (IgG) (Figure 2C). This signified *in vivo* association of NME2 with telomeric DNA. No PCR amplification was found in the case of anti-NME1 ChIP.

NME2 physically interacts with TRF2

As a further test of *in vivo* association with telomere ends, we asked if NME2 co-precipitates with any established telomere-end binding protein. Co-immunoprecipitation using anti-NME2 antibody from the nuclear extract of HT-1080 and A549 cells followed by western blot analysis indicated that NME2 physically associates with established TRF2 (Figure 3A–C and Supplementary Figure S2A). To validate the interaction we used anti-TRF2 antibody for immunoprecipitation from the nuclear extract of HT-1080 cells, where NME2 was detected in the immunoprecipitated fraction using anti-NME2 antibody (Figure 3B), confirming NME2-TRF2 interaction in the nucleus. NME2 interaction with TRF2 was further verified by *in vitro* pull-down from the nuclear lysate using His-tagged recombinant NME2 as bait, and the pull-down fraction was probed using anti-TRF2 antibody (Figure 3C). Enrichment of TRF2 was observed in fractions obtained from pull-down using His-tagged NME2 relative to Ni-NTA beads only (Figure 3C).

To test the possibility that NME2 interaction with TRF2 is DNA-dependent and/or NME2/TRF2 co-purify with telomeric DNA, we repeated the co-immunoprecipitation experiments in the presence of DNAse I or ethidium bromide (for intercalation of double-strand DNA) using anti-NME2 antibody and probed with anti-TRF2 antibody. NME2-TRF2 interaction was observed in both cases after treatment with DNAse I or ethidium bromide, indicating that DNA binding of NME2 was not essential for NME2-TRF2 association (Figure 3D and Supplementary Figure S2B). Recently, it was reported that telomeric repeat DNA is transcribed, which is known as telomeric repeat-containing RNA (TERRA) (38). Therefore, we further tested whether RNA was necessary for NME2 interaction with TRF2. Co-immunoprecipitation in the presence of RNAse-A did not affect NME2–TRF2 interactions. Therefore, it is unlikely that DNA/RNA binding (or any co-purifying nucleic acids) promotes association between NME2 and TRF2. Together, though these results support NME2–TRF2 association, they do not preclude involvement of another protein in assisting the interaction.

We also checked for intracellular co-localization of NME2 with TRF2 and found that NME2 localizes with TRF2 within the nucleus in HT-1080 (Supplementary Figure S3). However, though TRF2 immunofluorescence was distinct, we noted that NME2 staining inside cells was diffuse in nature, as was found in reports by several groups earlier (39–43). This appears to be an inherent characteristic of NME2, which limits the use of the immunofluorescence co-localization method in the case of NME2.

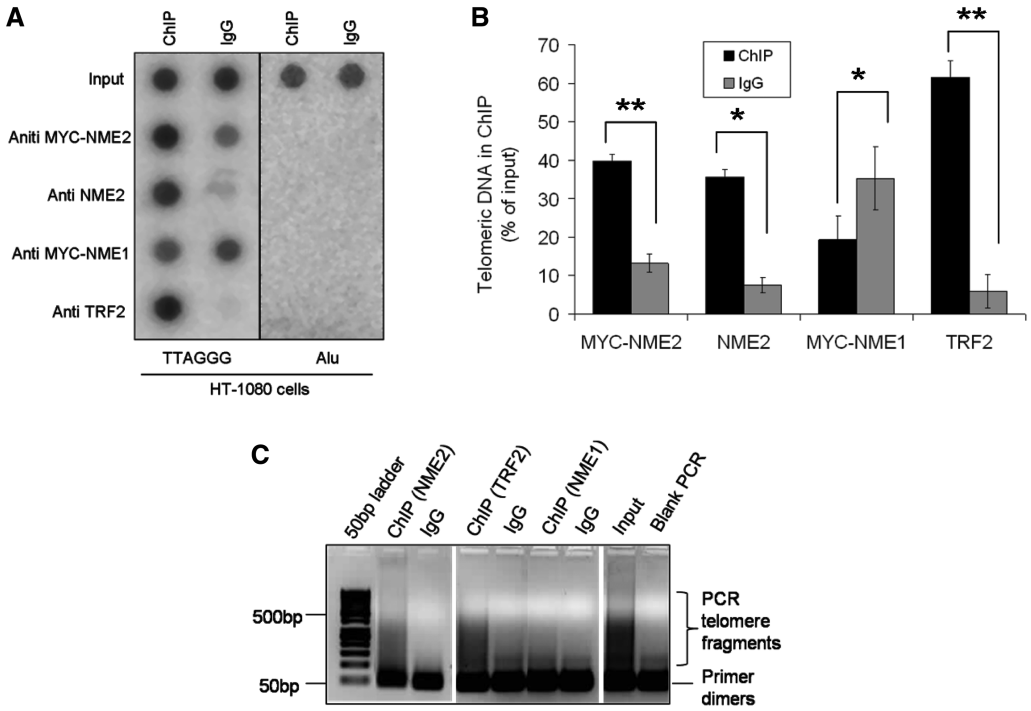

Figure 2. NME2 associates with telomere ends. (**A** and **B**) Immunoprecipitated DNA using anti-NME2, -TRF2, -MYC or specific isotype was hybridized with telomere-specific double strand or Alu sequence using dot blot (A). Quantification of TTAGGG repeat DNA recovered in each ChIP is shown in (B). Results are average of experiments performed in triplicate; $^{**}P < 0.01$, $^{*}P < 0.05$. (**C**) ChIP-PCR of immunoprecipitated DNA with probes specific for telomeric region. PCR amplified telomere fragments migrated as a smear (50 to ~500 bp); primer dimers migrated as a single band [as observed in blank (water)]. TRF2 ChIP was used as a positive control in both the cases.

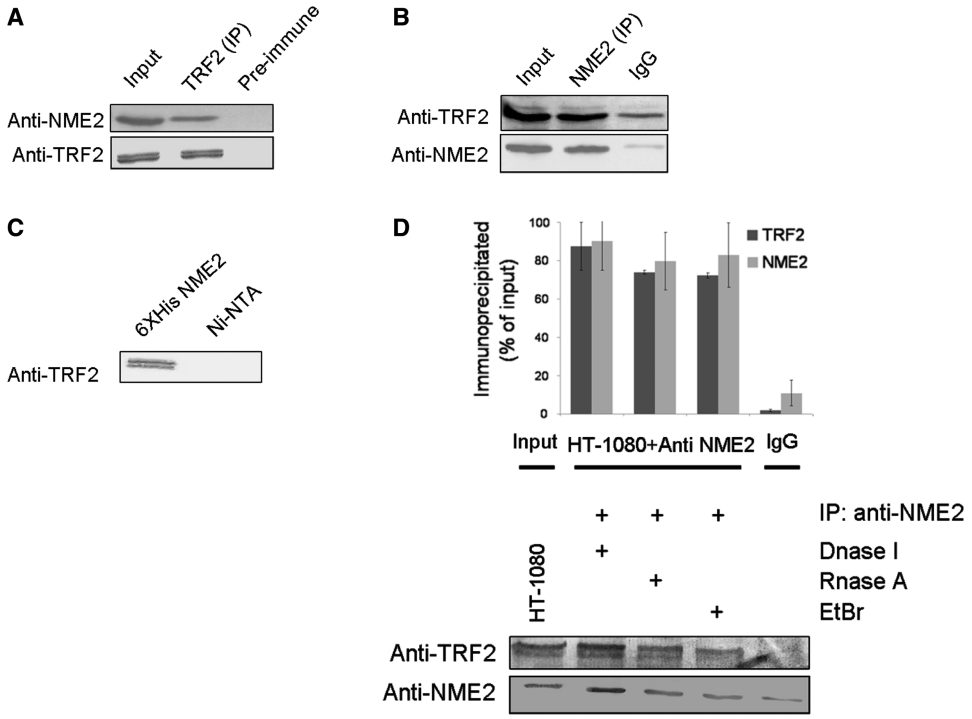

Figure 3. NME2 interacts with telomere binding factor TRF2. (**A**) Co-immunoprecipitation of NME2 with TRF2. HT-1080 nuclear lysate immunoprecipitated with anti-TRF2 antibody, followed by immunoblotting with anti-NME2 or anti-TRF2 antibody. (**B**) Reverse co-immunoprecipitation TRF2 by NME2. HT-1080 nuclear lysate immunoprecipitated with anti-NME2 or specific isotype and immunoblotted with anti-TRF2 or anti-NME2 antibody. (**C**) Interaction of NME2 with TRF2 *in vitro*. Ni-NTA only or Ni-NTA NME2 (purified his-tagged) beads were incubated with cell extracts from HT-1080 following by detection of bound TRF2 by immunoblot using TRF2-specific antibody. (**D**) Association of TRF2 and NME2 in HT-1080 cells was not affected after treatment with DNase I, ethidiumbromide (EtBr) or RNase A. Quantification is shown for IP with anti-TRF2 and anti-NME2 antibodies with respect to respective input fractions; average of three independent pull-down experiments is shown.

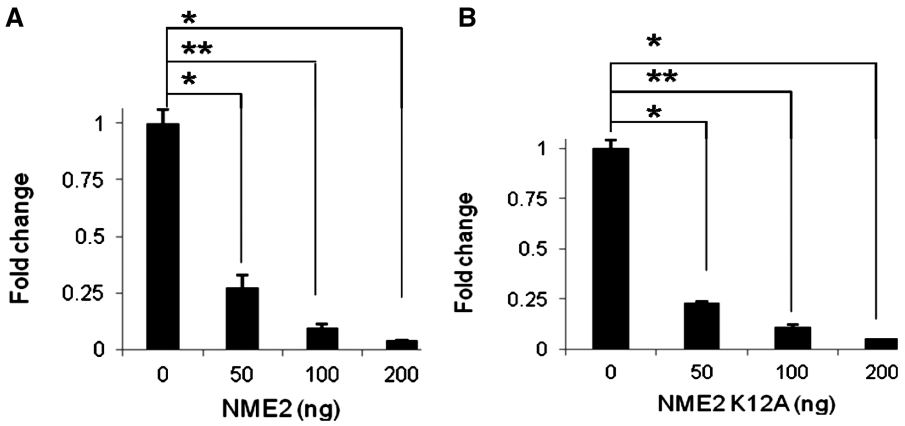

Figure 4. Inhibition of telomerase catalytic activity by NME2. Real time quantification of change in telomerase activity with respect to that at 0 ng NME2 is shown for either His-tag NME2 (**A**) or His-tag NME2 (K12A) (**B**) after incubating with telomerase extracts from HT-1080 cells for 10 min at 30°C. All experiments were performed in triplicate. $^{**}P < 0.01$, $^{*}P < 0.05$.

NME2 inhibits telomerase activity *in vitro*

To question the relevance of NME2 association with telomere ends, we focused on testing whether NME2 had any influence on telomerase activity. Quantification of telomerase activity (real-time monitoring of the TRAP assay product) in the presence of NME2 gave a dose-dependent decrease in telomerase catalytic activity in cell lysates prepared from HT-1080 (Figure 4A). Increasing amount of purified recombinant His-tagged NME2 was used. These results showed that NME2 negatively affects the typical 6-nt ladder of primer extension products characteristic of human telomerase. Nuclease activity of NME2 has been reported (44), and therefore inhibition of telomerase extension could result from cleavage of template DNA required for telomerase extension. This was checked using recombinant His-tagged mutant $NME2^{K12A}$, which is devoid of cleavage activity (28). Telomerase inhibition by $NME2^{K12A}$ was very similar to that obtained for wild-type NME2 (Figure 4B), indicating that telomerase inhibition was unlikely to result from DNA cleavage. In order to ensure the specificity of telomerase inactivation by NME2/NME2 (K12A), we used similar concentrations of bovine serum albumin (BSA) as a non-specific control and found there was no inhibition of telomerase activity (Supplementary Figure S5).

NME2 associates with telomerase

Next we sought to ask whether NME2 associates with telomerase. In co-immunoprecipitation experiments performed with nuclear extract of HT-1080 and A549 cells, hTERT was readily detected by western blot in the immunoprecipitated anti-NME2 fraction, but not in the isotype control (IgG) (Figure 5A and Supplementary Figure S6A). Conversely, on using anti-hTERT antibody for immunoprecipitation from nuclear extract of HT-1080 cells, NME2 was detected in the immunoprecipitated fraction using anti-NME2 antibody (Figure 5B). In order to test the interaction more specifically, we used HA-tagged hTERT, and NME2 was readily detected by western blot in the fraction immunoprecipitated with anti-HA antibody, but not in the isotype control (Figure 5C). Further confirmation of this interaction was gained from *in vitro* pull-down assay. Using His-tagged NME2 as the bait protein, we were able to extract hTERT from the nuclear extract (Figure 5D). In addition to this, we performed immunofluorescence microscopy to test NME2 localization with hTERT within the nucleus (Supplementary Figure S3). However, as mentioned above we found that NME2 distribution in the nucleus was diffuse while hTERT occupancy was distinct.

Keeping in mind that NME2 associates with telomeric DNA, it is possible that NME2 interaction with telomerase is DNA-dependent and/or NME2/telomerase co-purify with telomeric DNA. To check this possibility we repeated the co-immunoprecipitation reactions in the presence of DNAse I or ethidium bromide using anti-hTERT antibody and probed with anti-NME2 antibody. NME2-hTERT association was found to remain largely unaltered after treatment with DNAse I or ethidium bromide, though we noted some decrease in the case of DNase-I, and this was not significant (Figure 5D and Supplementary Figure S6B); also, pull-down efficiency was similar in all cases (lower panel). We further tested whether involvement of the RNA component of telomerase (hTERC) was essential. Co-immunoprecipitation in the presence of RNAse-A again did not affect NME2-hTERT association significantly, suggesting that the RNA component of telomerase may not be essential for NME2-hTERT association. However, this does not exclude the role of telomerase-bound hTERC that may not be amenable to RNase-A digestion. Together, though these results support the possibility that DNA/RNA binding is not necessary, it does not rule out the role of other proteins in NME2-hTERT association.

Sustained NME2 expression results in reduced telomerase activity and telomere length *in vivo*

Based on the finding that NME2 inhibits telomerase activity *in vitro*, we next sought to check whether NME2 influenced telomere length and/or telomerase activity

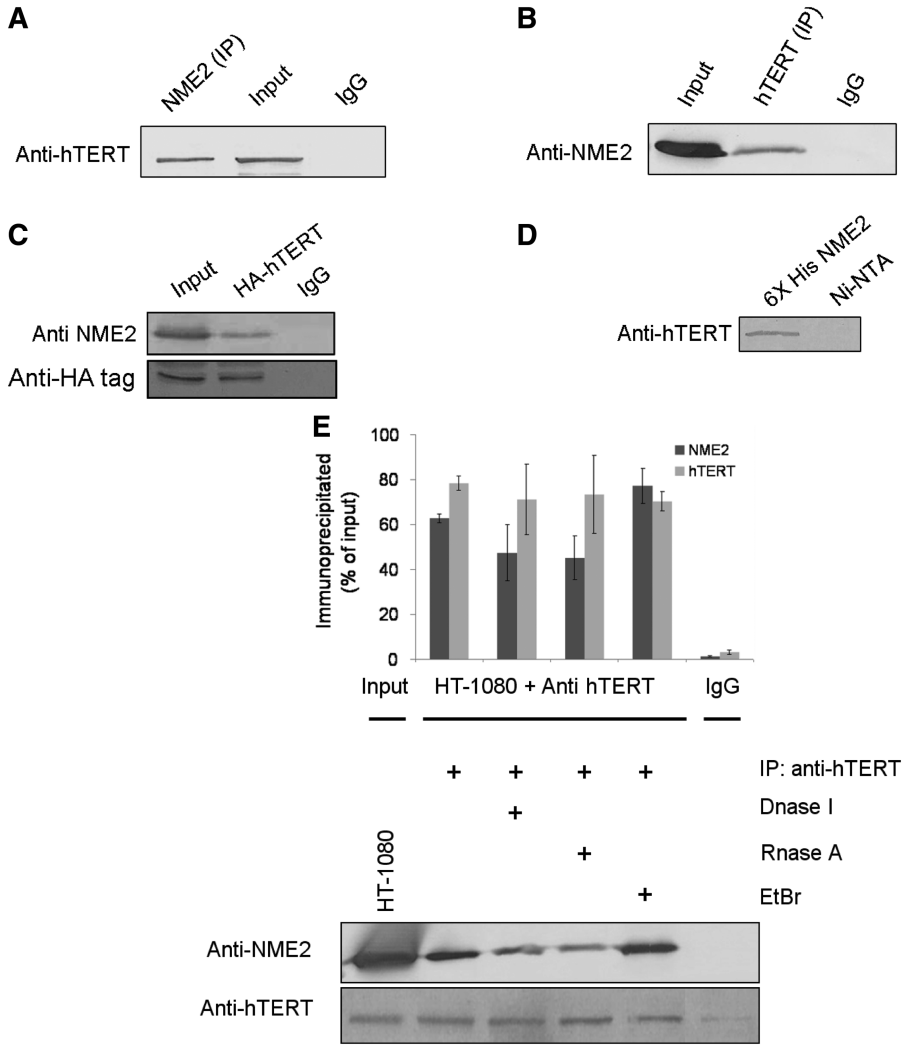

Figure 5. NME2 directly interacts with hTERT (**A–C**). Co-immunoprecipitation of NME2 and hTERT. HT-1080 nuclear lysate was subjected to immunoprecipitation with anti-NME2 (A), -hTERT (B), -HA-hTERT (C) antibody, followed by immunoblotting with either anti-hTERT, anti-NME2 or anti-HA-tag antibody (A, B, C, respectively). (**D**) Interaction of NME2 with hTERT *in vitro*. Ni-NTA only or Ni-NTA NME2 (His-tagged) beads were incubated with cell extracts from HT-1080 following by detection of bound hTERT by immunoblot using anti-hTERT antibody. (**E**) Association of endogenous hTERT with NME2 in HT-1080 cells was not changed after treatment with DNase I, ethidiumbromide (EtBr) or RNase A. Quantification is shown for IP with anti-NME2 and anti-hTERT antibodies with respect to respective input fractions; average of three independent pull-down experiments is shown.

in vivo. In order to check this, HT 1080 cells with stable expression of HA-tagged NME2 (Figure 6A and B) were generated and the fluorescence-based FLOW-FISH method (45, 46) was used to quantify telomere length relative to cells that were transformed in a similar manner with the HA-tag vector backbone lacking NME2. Reduced telomere length relative to vector-transformed cells was observed across increasing population doubling times (Figure 6C). Consistent with this, we found a marked reduction of telomerase activity (real-time TRAP assay) in cells expressing NME2 compared to vector-transformed cells (Figure 6D), in line with the *in vitro* results showing inhibition of telomerase activity in the presence of NME2. It is possible that reduced telomerase activity was due to lower levels of hTERT expression. Therefore, we checked telomerase levels. NME2-expressing stable cells showed no significant change in hTERT transcript and protein levels relative to the vector-transformed cells (Figure 6E and F).

DISCUSSION

Several aspects of the findings presented here demonstrate novel biological functions of NME2 related to telomere/telomerase interactions. First, using a novel method of analyzing ChIP-sequencing short-read data we found that NME2 localizes at telomere ends *in vivo*; as further support of its presence at telomere ends, NME2 was found to physically associate with the telomeric double-strand binding factor TRF2. Second, our findings reveal NME2 interaction with telomerase and demonstrate that NME2 negatively regulates telomerase activity *in vitro* and *in vivo*. Finally, we observed that telomere length was reduced in

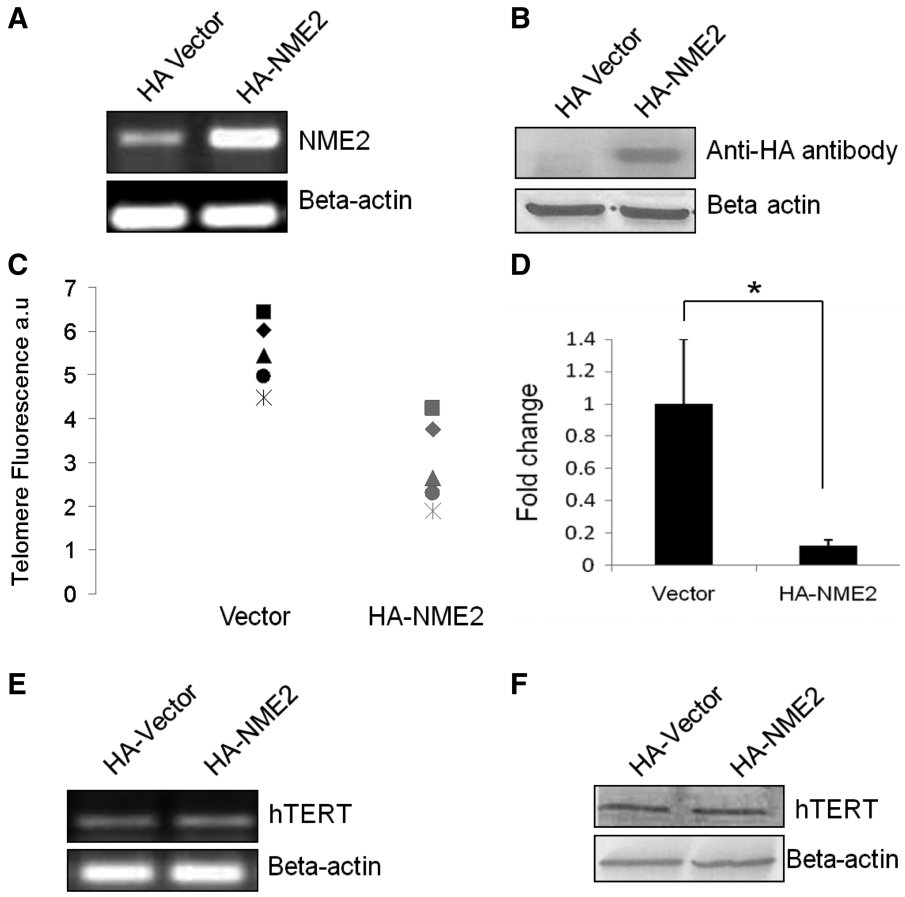

Figure 6. Sustained expression of NME2 decreases telomere length. (**A** and **B**) RT-PCR (A) and western blot (B) for stable expression of HA-tagged NME2 in HT-1080 cells. (**C**) Flow-FISH analysis of telomere length in HA-NME2 cells compared to HA-vector cells with increasing population doubling time [each point represent 10 000 cells from population doubling time points: closed squares, 45, closed diamonds, 90, closed triangles, 130, closed circles, 170 and asterisk 200)]; three independent experiments were performed, a representative analysis is shown. (**D**) Telomerase activity in HA-NME2 cells using real time quantification of telomerase activity; $*P < 0.05$. (**E** and **F**) RT–PCR (E) and western blot analysis (F) shows no change in hTERT level in HA-NME2 expressing cells.

cells with sustained expression of NME2 relative to vector-control cells. To the best of our knowledge, *in vivo* association of NME2 with telomeres, TRF2 or telomerase, including NME2-mediated reduction in telomerase activity and telomere length in cancer cells have not been reported before.

One earlier study reported that recombinant NME2 binds to short telomeric oligonucleotides and influences telomerase activity *in vitro* (however, we noted that an unusually high amount of NME2 was used) (47). Our findings, on the other hand, are based on the initial finding that NME2 associates with telomere ends *in vivo* (ChIP-seq and other experiments). Furthermore, telomerase activity and telomere length measurements performed *in vivo* using cells modified for sustained NME2 expression complement the initial findings and demonstrate a novel function of NME2.

It has been reported earlier that NME2 occupies the nuclei specifically in S-phase and not in the M-phase (48). This is consistent with the likely role of NME2 in this context, as telomere synthesis and related regulatory activities occur primarily during the S-phase. A recent paper that identified all proteins associated with telomeres using a high-throughput method did not find NME2 (49). Though reasons for this are not clear to us, considering the S-phase-specific localization of NME2 it is possible that NME2-telomere association is transient in nature, limiting identification by high-throughput methods.

Apart from the reported NME2 ChIP-seq peaks harbouring telomeric repeat units we found many instances of binding positions with two to four contiguous repeating units. We believe this results from sub-telomeric regions where interspersed TTAGGG repeats have been noted earlier (50). In line with this we also noted several peaks that resulted from regions distant from telomere ends (Supplementary Table S2A and S2B). Together, this suggests that NME2 recognizes telomeric repeat sequences irrespective of their position within the genome.

Correlation between telomerase levels and progression of metastasis have been reported (12, 14). Ribozyme-mediated suppression of mouse telomerase RNA gave decreased telomerase expression and telomerase activity in B16-F10 murine melanoma resulting in reduced tumour invasion and metastatic potential (14). On the

other hand, reduced telomeric DNA content was found to adversely affect breast cancer-free survival (51), indicating the complexity of telomeres/telomerase in relation to cancer progression (52). Interestingly, a recent study demonstrated that the contrasting observations regarding tumour-suppressive and -promoting potential of telomere-shortening could be due to the status of the tumour suppressor p53 (53). In this context, it is interesting to consider that telomere length/telomerase activity may play a key role in metastatic progression. Findings reported here showing NME2, a metastases suppressor, as a potential regulator of telomerase activity suggest the possibility that NME2 negatively influences metastatic invasion by controlling telomerase activity.

Although our data demonstrate NME2 as a telomere binding factor that associates with and modulates telomerase activity *in vivo*, further work is required to understand the implications of NME2-mediated telomere transactions with reference to metastases suppression. For example, it will be interesting to study the mechanisms of how NME2 may function as a connection between telomere length alteration and metastatic progression of cancer cells. To our knowledge this is the first evidence directly connecting any metastases suppressor to the telomere machinery in a cellular context.

SUPPLEMENTARY DATA

Supplementary Data are available at NAR Online: Suplementary Method, Supplementary Tables 1–3 and Supplementary Figures 1–6.

ACKNOWLEDGEMENTS

All molecular experiments were performed by A.K., G.P., D.S. and A.S.; ChIP-seq experiments were performed by D.S., A.S. and R.K.T; ChIP-seq analysis was performed by V.Y., P.D. and P.K.; manuscript was written by A.K. with help from S.C. We thank Rajkumar Sunil Singh (TCGA) for technical assistance in imaging and Atul Ranjan and Mohd. Parwez Alam (ACBR) for help with dot blot experiments.

FUNDING

Department of Biotechnology (to A.K.); Department of Science and Technology (to G.P. and D.S.); Council of Scientific and Industrial Research (to V.Y., R.K.T. and S.C.); Council of Scientific and Industrial Research (CMM0017 to A.S. and SIP06 to P.K.); European Community's Seventh Framework Programme, GEN2PHEN project (200754 to P.K.); Department of Biotechnology (PR6752 to S.C.). Funding for open access charge: Waived by Oxford University Press.

Conflict of interest statement. None declared.

REFERENCES

1. Blackburn,E.H. (1991) Structure and function of telomeres. *Nature*., **350**, 569–573.
2. Palm,W. and de,L.T. (2008) How shelterin protects mammalian telomeres. *Annu. Rev. Genet*., **42**, 301–334.
3. de Lange,T. (2005) Shelterin: the protein complex that shapes and safeguards human telomeres. *Genes Dev*., **19**, 2100–2110.
4. Liu,D., O'Connor,M.S., Qin,J. and Songyang,Z. (2004) Telosome, a mammalian telomere-associated complex formed by multiple telomeric proteins. *J. Biol. Chem*., **279**, 51338–51342.
5. Greider,C.W. (1996) Telomere length regulation. *Annu. Rev. Biochem*., **65**, 337–365.
6. Martinez,P. and Blasco,M.A. (2010) Role of shelterin in cancer and aging. *Aging Cell*, **9**, 653–666.
7. Lansdorp,P.M. (2009) Telomeres and disease. *EMBO J*., **28**, 2532–2540.
8. Blackburn,E.H. (1992) Telomerases. *Annu. Rev. Biochem*., **61**, 113–129.
9. Lingner,J. and Cech,T.R. (1996) Purification of telomerase from *Euplotes aediculatus*: requirement of a primer 3′ overhang. *Proc. Natl Acad. Sci. USA*, **93**, 10712–10717.
10. Artandi,S.E. and DePinho,R.A. (2010) Telomeres and telomerase in cancer. *Carcinogenesis*, **31**, 9–18.
11. Chang,S., Khoo,C.M., Naylor,M.L., Maser,R.S. and DePinho,R.A. (2003) Telomere-based crisis: functional differences between telomerase activation and ALT in tumor progression. *Genes Dev*., **17**, 88–100.
12. Nosrati,M., Li,S., Bagheri,S., Ginzinger,D., Blackburn,E.H., Debs,R.J. and Kashani-Sabet,M. (2004) Antitumor activity of systemically delivered ribozymes targeting murine telomerase RNA. *Clin. Cancer Res*., **10**, 4983–4990.
13. Takada,T., Hayashi,T., Arakawa,M. and Kominami,R. (1992) Telomere elongation frequently observed during tumor metastasis. *Jpn. J. Cancer Res*., **83**, 1124–1127.
14. Bagheri,S., Nosrati,M., Li,S., Fong,S., Torabian,S., Rangel,J., Moore,D.H., Federman,S., Laposa,R.R., Baehner,F.L. *et al.* (2006) Genes and pathways downstream of telomerase in melanoma metastasis. *Proc. Natl Acad. Sci. USA*, **103**, 11306–11311.
15. Steeg,P.S., Cohn,K.H. and Leone,A. (1991) Tumor metastasis and nm23: current concepts. *Cancer Cells*, **3**, 257–262.
16. Bilitou,A., Watson,J., Gartner,A. and Ohnuma,S. (2009) The NM23 family in development. *Mol. Cell Biochem*., **329**, 17–33.
17. Steeg,P.S., Zollo,M. and Wieland,T. (2011) A critical evaluation of biochemical activities reported for the nucleoside diphosphate kinase/Nm23/Awd family proteins: opportunities and missteps in understanding their biological functions. *Naunyn Schmiedebergs Arch. Pharmacol*., **384**, 331–339.
18. Mehta,A. and Orchard,S. (2009) Nucleoside diphosphate kinase (NDPK, NM23, AWD): recent regulatory advances in endocytosis, metastasis, psoriasis, insulin release, fetal erythroid lineage and heart failure; translational medicine exemplified. *Mol. Cell Biochem*., **329**, 3–15.
19. Boissan,M., Dabernat,S., Peuchant,E., Schlattner,U., Lascu,I. and Lacombe,M.L. (2009) The mammalian Nm23/NDPK family: from metastasis control to cilia movement. *Mol. Cell Biochem*., **329**, 51–62.
20. Lo,M.L., Mignogna,M.D., Pannone,G., Staibano,S., Procaccini,M., Serpico,R., De,R.G. and Scully,C. (1999) The NM23 gene and its expression in oral squamous cell carcinoma. *Oncol. Rep*., **6**, 747–751.
21. Baba,H., Urano,T., Okada,K., Furukawa,K., Nakayama,E., Tanaka,H., Iwasaki,K. and Shiku,H. (1995) Two isotypes of murine nm23/nucleoside diphosphate kinase, nm23-M1 and nm23-M2, are involved in metastatic suppression of a murine melanoma line. *Cancer Res*., **55**, 1977–1981.
22. Russell,R.L., Pedersen,A.N., Kantor,J., Geisinger,K., Long,R., Zbieranski,N., Townsend,A., Shelton,B., Brunner,N. and Kute,T.E. (1998) Relationship of nm23 to proteolytic factors, proliferation and motility in breast cancer tissues and cell lines. *Br. J. Cancer*, **78**, 710–717.
23. Thakur,R.K., Yadav,V.K., Kumar,P. and Chowdhury,S. (2011) Mechanisms of non-metastatic 2 (NME2)-mediated control of

metastasis across tumor types. *Naunyn Schmiedebergs Arch. Pharmacol*, **384**, 397–406.
24. Nelson,J.D., Denisenko,O. and Bomsztyk,K. (2006) Protocol for the fast chromatin immunoprecipitation (ChIP) method. *Nat. Protoc.*, **1**, 179–185.
25. Li,H., Ruan,J. and Durbin,R. (2008) Mapping short DNA sequencing reads and calling variants using mapping quality scores. *Genome Res.*, **18**, 1851–1858.
26. Ji,H., Jiang,H., Ma,W., Johnson,D.S., Myers,R.M. and Wong,W.H. (2008) An integrated software system for analyzing ChIP-chip and ChIP-seq data. *Nat. Biotechnol.*, **26**, 1293–1300.
27. Birney,E., Stamatoyannopoulos,J.A., Dutta,A., Guigo,R., Gingeras,T.R., Margulies,E.H., Weng,Z., Snyder,M., Dermitzakis,E.T., Thurman,R.E. *et al.* (2007) Identification and analysis of functional elements in 1% of the human genome by the ENCODE pilot project. *Nature*, **447**, 799–816.
28. Thakur,R.K., Kumar,P., Halder,K., Verma,A., Kar,A., Parent,J.L., Basundra,R., Kumar,A. and Chowdhury,S. (2009) Metastases suppressor NM23-H2 interaction with G-quadruplex DNA within c-MYC promoter nuclease hypersensitive element induces c-MYC expression. *Nucleic Acids Res.*, **37**, 172–183.
29. Kharchenko,P.V., Tolstorukov,M.Y. and Park,P.J. (2008) Design and analysis of ChIP-seq experiments for DNA-binding proteins. *Nat. Biotechnol.*, **26**, 1351–1359.
30. Berberich,S.J. and Postel,E.H. (1995) PuF/NM23-H2/NDPK-B transactivates a human c-myc promoter-CAT gene via a functional nuclease hypersensitive element. *Oncogene*, **10**, 2343–2347.
31. Dexheimer,T.S., Carey,S.S., Zuohe,S., Gokhale,V.M., Hu,X., Murata,L.B., Maes,E.M., Weichsel,A., Sun,D., Meuillet,E.J. *et al.* (2009) NM23-H2 may play an indirect role in transcriptional activation of c-myc gene expression but does not cleave the nuclease hypersensitive element III(1). *Mol. Cancer Ther.*, **8**, 1363–1377.
32. Postel,E.H., Mango,S.E. and Flint,S.J. (1989) A nuclease-hypersensitive element of the human c-myc promoter interacts with a transcription initiation factor. *Mol. Cell Biol.*, **9**, 5123–5133.
33. Postel,E.H., Berberich,S.J., Rooney,J.W. and Kaetzel,D.M. (2000) Human NM23/nucleoside diphosphate kinase regulates gene expression through DNA binding to nuclease-hypersensitive transcriptional elements. *J. Bioenerg. Biomembr.*, **32**, 277–284.
34. Auerbach,R.K., Euskirchen,G., Rozowsky,J., Lamarre-Vincent,N., Moqtaderi,Z., Lefrancois,P., Struhl,K., Gerstein,M. and Snyder,M. (2009) Mapping accessible chromatin regions using Sono-Seq. *Proc. Natl Acad. Sci. USA*, **106**, 14926–14931.
35. Rozowsky,J., Euskirchen,G., Auerbach,R.K., Zhang,Z.D., Gibson,T., Bjornson,R., Carriero,N., Snyder,M. and Gerstein,M.B. (2009) PeakSeq enables systematic scoring of ChIP-seq experiments relative to controls. *Nat. Biotechnol.*, **27**, 66–75.
36. Cawthon,R.M. (2002) Telomere measurement by quantitative PCR. *Nucleic Acids Res.*, **30**, e47.
37. Gomez,D., O'Donohue,M.F., Wenner,T., Douarre,C., Macadre,J., Koebel,P., Giraud-Panis,M.J., Kaplan,H., Kolkes,A., Shin-ya,K. *et al.* (2006) The G-quadruplex ligand telomestatin inhibits POT1 binding to telomeric sequences in vitro and induces GFP-POT1 dissociation from telomeres in human cells. *Cancer Res.*, **66**, 6908–6912.
38. Azzalin,C.M., Reichenbach,P., Khoriauli,L., Giulotto,E. and Lingner,J. (2007) Telomeric repeat containing RNA and RNA surveillance factors at mammalian chromosome ends. *Science*, **318**, 798–801.
39. Fournier,H.N., Dupe-Manet,S., Bouvard,D., Lacombe,M.L., Marie,C., Block,M.R. and biges-Rizo,C. (2002) Integrin cytoplasmic domain-associated protein 1alpha (ICAP-1alpha) interacts directly with the metastasis suppressor nm23-H2, and both proteins are targeted to newly formed cell adhesion sites upon integrin engagement. *J. Biol. Chem.*, **277**, 20895–20902.
40. Fournier,H.N., biges-Rizo,C. and Block,M.R. (2003) New insights into Nm23 control of cell adhesion and migration. *J. Bioenerg. Biomembr.*, **35**, 81–87.
41. Gallagher,B.C., Parrott,K.A., Szabo,G. and de Otero,S. (2003) Receptor activation regulates cortical, but not vesicular localization of NDP kinase. *J. Cell Sci.*, **116**, 3239–3250.
42. Pinon,V.P., Millot,G., Munier,A., Vassy,J., Linares-Cruz,G., Capeau,J., Calvo,F. and Lacombe,M.L. (1999) Cytoskeletal association of the A and B nucleoside diphosphate kinases of interphasic but not mitotic human carcinoma cell lines: specific nuclear localization of the B subunit. *Exp. Cell Res.*, **246**, 355–367.
43. Rochdi,M.D., Laroche,G., Dupre,E., Giguere,P., Lebel,A., Watier,V., Hamelin,E., Lepine,M.C., Dupuis,G. and Parent,J.L. (2004) Nm23-H2 interacts with a G protein-coupled receptor to regulate its endocytosis through an Rac1-dependent mechanism. *J. Biol. Chem.*, **279**, 18981–18989.
44. Postel,E.H., Abramczyk,B.A., Gursky,S.K. and Xu,Y. (2002) Structure-based mutational and functional analysis identify human NM23-H2 as a multifunctional enzyme. *Biochemistry*, **41**, 6330–6337.
45. Baerlocher,G.M., Vulto,I., de,J.G. and Lansdorp,P.M. (2006) Flow cytometry and FISH to measure the average length of telomeres (flow FISH). *Nat. Protoc.*, **1**, 2365–2376.
46. Baerlocher,G.M., Mak,J., Tien,T. and Lansdorp,P.M. (2002) Telomere length measurement by fluorescence in situ hybridization and flow cytometry: tips and pitfalls. *Cytometry*, **47**, 89–99.
47. Nosaka,K., Kawahara,M., Masuda,M., Satomi,Y. and Nishino,H. (1998) Association of nucleoside diphosphate kinase nm23-H2 with human telomeres. *Biochem. Biophys. Res. Commun.*, **243**, 342–348.
48. Kraeft,S.K., Traincart,F., Mesnildrey,S., Bourdais,J., Veron,M. and Chen,L.B. (1996) Nuclear localization of nucleoside diphosphate kinase type B (nm23-H2) in cultured cells. *Exp. Cell Res.*, **227**, 63–69.
49. Dejardin,J. and Kingston,R.E. (2009) Purification of proteins associated with specific genomic Loci. *Cell*, **136**, 175–186.
50. Flint,J., Bates,G.P., Clark,K., Dorman,A., Willingham,D., Roe,B.A., Micklem,G., Higgs,D.R. and Louis,E.J. (1997) Sequence comparison of human and yeast telomeres identifies structurally distinct subtelomeric domains. *Hum. Mol. Genet.*, **6**, 1305–1313.
51. Heaphy,C.M., Baumgartner,K.B., Bisoffi,M., Baumgartner,R.N. and Griffith,J.K. (2007) Telomere DNA content predicts breast cancer-free survival interval. *Clin. Cancer Res.*, **13**, 7037–7043.
52. Artandi,S.E. (2003) Complex roles for telomeres and telomerase in breast carcinogenesis. *Breast Cancer Res.*, **5**, 37–41.
53. Perera,S.A., Maser,R.S., Xia,H., McNamara,K., Protopopov,A., Chen,L., Hezel,A.F., Kim,C.F., Bronson,R.T., Castrillon,D.H. *et al.* (2008) Telomere dysfunction promotes genome instability and metastatic potential in a K-ras p53 mouse model of lung cancer. *Carcinogenesis*, **29**, 747–753.